

Think Parallax: Solving Multi-Hop Problems via Multi-View Knowledge-Graph-Based Retrieval-Augmented Generation

Jinliang Liu^{1,2}, Jiale Bai¹, Shaoning Zeng^{1,2*}

¹School of Information and Software Engineering, UESTC, Chengdu, Sichuan, China

²Yangtze Delta Region Institute (Huzhou), UESTC, Huzhou, Zhejiang, China

lucaliu510@gmail.com, syxb02@gmail.com, zsn@outlook.com

Abstract

Large language models (LLMs) still struggle with multi-hop reasoning over knowledge-graphs (KGs), and we identify a previously overlooked structural reason for this difficulty: Transformer attention heads naturally specialize in distinct semantic relations across reasoning stages, forming a hop-aligned relay pattern. This key finding suggests that multi-hop reasoning is inherently multi-view, yet existing KG-based retrieval-augmented generation (KG-RAG) systems collapse all reasoning hops into a single representation, flat embedding space, suppressing this implicit structure and causing noisy or drifted path exploration. We introduce ParallaxRAG, a symmetric multi-view framework that decouples queries and KGs into aligned, head-specific retrieval spaces. By enforcing relational diversity across heads while constraining weakly related paths, ParallaxRAG constructs more accurate, cleaner subgraphs and guides LLMs through grounded, hop-wise reasoning. On WebQSP and CWQ, it achieves state-of-the-art retrieval and QA performance, substantially reduces hallucination, and generalizes strongly to the biomedical BioASQ benchmark. Our implementation is available at <https://anonymous.4open.science/r/ParallaxRAG-2743>.

1 Introduction

Multi-hop reasoning over KGs remains a central challenge for LLMs. Although RAG improves factual grounding (Lewis et al., 2020), existing KG-RAG systems still struggle with long reasoning chains (Luo et al., 2023), compounding errors (Mavromatis and Karypis, 2024), and the rapid expansion of irrelevant graph paths (He et al., 2024). These issues limit both the accuracy and robustness of downstream question answering.

Our analysis identifies an architectural property of Transformers that is directly relevant to this problem: different attention heads consistently specialize in distinct semantic relations across reasoning stages, forming a hop-aligned pattern. Early heads emphasize local or entity-level relations, whereas later heads capture more abstract or compositional dependencies. This observation suggests that multi-hop reasoning is inherently multi-view, with different hops requiring distinct representational subspaces.

Current KG-RAG approaches do not leverage this structure. Most methods encode queries and graph triples into a single embedding space (Fu et al., 2020; Ji et al., 2021), which conflates hop-specific semantics and hinders step-wise reasoning. This monolithic representation causes early-hop signals to interfere with deeper relational composition, increasing noise and reducing retrieval precision (Liu et al., 2023). Iterative LLM-based reasoning (Sun et al., 2023) offers partial improvements but introduces high latency and lacks an explicit mechanism for hop decomposition over KGs. These limitations indicate a structural mismatch: multi-hop reasoning requires hop-separated semantics, yet existing KG-RAG systems enforce a single shared embedding basis.

To instantiate this principle, we introduce ParallaxRAG, a framework based on symmetric multi-head decoupling. We leverage transformer multi-head activations to decompose queries into multi-view representations (Vaswani et al., 2017; Besta et al., 2024), while projecting KG triples into aligned multi-faceted latent spaces (Mavromatis and Karypis, 2024; Li et al., 2024). Two mechanisms operationalize this framework: (1) a Pairwise Similarity Regularization (PSR) module integrated into the Distance Encoding (DE) stage, which enforces head-level specialization and prevents repre-

*Corresponding author

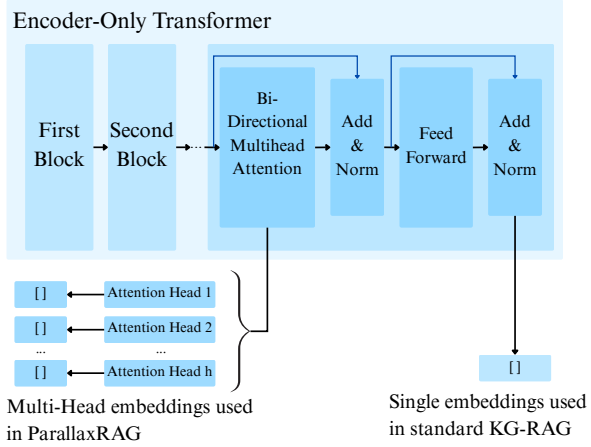


Figure 1: Comparison of standard KG-RAG and multi-head KG-RAG embeddings. In ParallaxRAG, attention heads specialize in distinct semantic relations across reasoning stages, contributing to successive hops in the reasoning chain.

sentential collapse; and (2) a lightweight retrieval component that consolidates head-specific information to reduce noise and improve alignment between queries and graph structure (Khattab and Zaharia, 2020).

Our main contributions are as follows:

- **Multi-head decoupling architecture for KG-RAG.** We propose the first KG-RAG framework that decouples queries and KGs into head-specific views, allowing attention heads to capture complementary relational cues at different reasoning depths. A joint exploration-exploitation strategy—PSR and weakly supervised gating—enhances robustness and promotes specialization.
- **Head specialization in multi-hop reasoning.** We provide the first empirical evidence of a relay effect, where distinct head groups dominate different stages of multi-hop reasoning. New metrics quantify head-level contribution and effectiveness.
- **Strong and generalizable performance.** ParallaxRAG achieves state-of-the-art results on WebQSP and CWQ, and strong generalization performance on BioASQ. Under zero-shot transfer, it surpasses the previous SOTA by 7.32 Macro-F1, demonstrating highly transferable reasoning capabilities.

2 Related Work

2.1 Retrieval-Augmented Generation (RAG)

RAG grounds LLMs in external knowledge to mitigate hallucination (Lewis et al., 2020). Dense retrievers have shown strong results (Karpukhin et al., 2020; Izacard et al., 2022; Gao et al., 2023), but struggle with unstructured or redundant data (Izacard and Grave, 2020; Petroni et al., 2020). KG-RAG leverages structured KGs (Peng et al., 2024), yet most methods focus on fact lookup. We instead emphasize query-graph representations to support complex, multi-hop reasoning (Khattab and Zaharia, 2020).

2.2 Multi-Head Embeddings

Multi-Head attention (MHA) variants have improved embeddings across modalities, e.g., visual-semantic alignment via self-attention (Park et al., 2020), redundancy reduction (Bhajanapalli et al., 2021; Bian et al., 2021), and low-resource multilingual tasks (Vashisht et al., 2025). In RAG, MRAG exploits MHA activations for multi-aspect retrieval (Besta et al., 2024). Our ParallaxRAG extends this idea with a synergistic framework, enabling an efficient MLP retriever to build concise, reasoning-ready subgraphs.

2.3 Multi-Hop QA

Two main lines exist: enhancing LLM reasoning via decomposition or prompting (Perez et al., 2020; Fu et al., 2021; Wei et al., 2022), and improving retrieval via iterative or adaptive methods (Trivedi et al., 2022; Asai et al., 2024). These typically require multiple LLM calls. Our approach instead leverages encoder-only Transformers, where multi-head attention naturally specializes in different hops or relations, yielding efficient multi-hop reasoning.

3 The ParallaxRAG Framework

Multi-hop reasoning over knowledge graphs requires connecting multiple relational steps in a consistent manner. However, most KG-RAG systems collapse this process into a single embedding space, which obscures step-wise structure. ParallaxRAG builds on the intuition that each reasoning hop should be represented from a distinct perspective. By decomposing both the query and the graph into multiple, aligned views, and regulating their interaction through a balanced exploration-exploitation process, ParallaxRAG retrieves

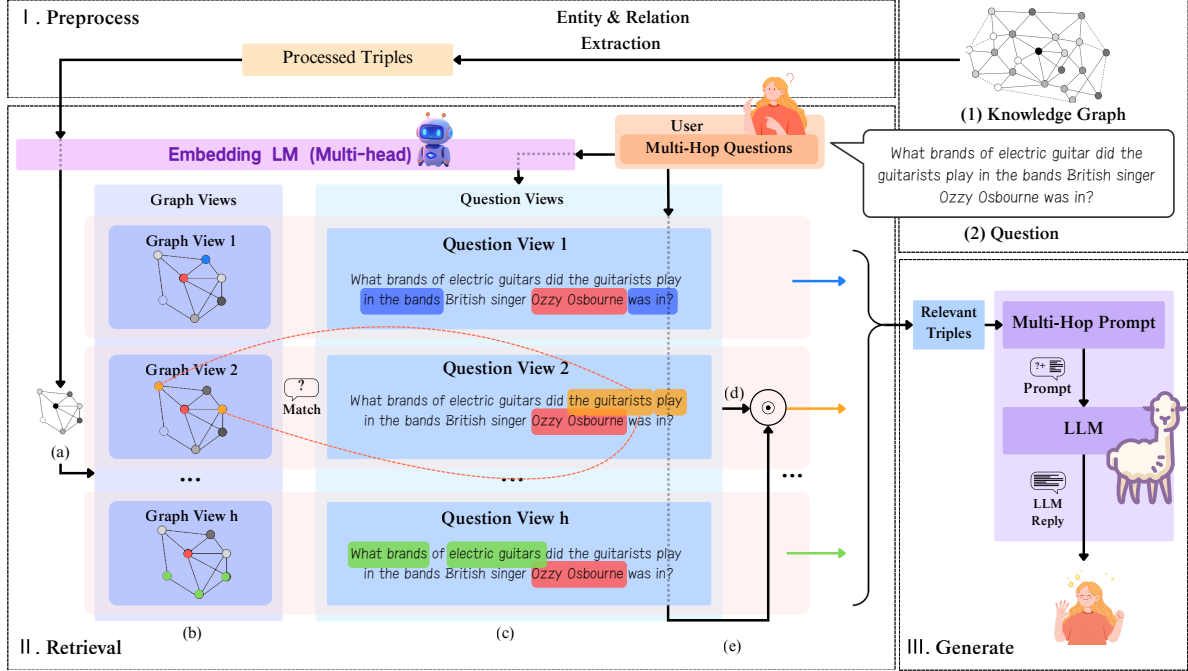


Figure 2: The architecture of ParallaxRAG, illustrating its three main stages: Preprocess, Retrieval, and Generate. The core retrieval process begins by creating specialized multi-view representations for both the graph (b) and the question (c), a process guided by directional distance encoding and regularized by pairwise similarity (a). Next, candidate triples are scored in parallel across these diverse views (d). Finally, a query-aware gating mechanism computes head importance (e) to produce a weighted aggregation of the scores, identifying the most relevant triples for the final generation stage.

compact, interpretable subgraphs that better support multi-hop reasoning.

3.1 Symmetric Decoupling of Query and Graph Views

In standard KG-RAG, a complex query is encoded as a single vector $\mathbf{q} \in \mathbb{R}^d$, conflating semantics required for different reasoning stages. We instead leverage the internal multi-head structure of a Transformer to obtain H specialized query views:

$$Q^{\text{views}} = \{\mathbf{q}_k \in \mathbb{R}^{d_h}\}_{k=1}^H.$$

On the graph side, each triple $\tau = (h, r, t)$ is symmetrically projected into the same H latent spaces, yielding head-specific representations $(\mathbf{e}_k, \mathbf{r}_k)$. This design aligns the query and the graph across multiple semantic dimensions—allowing each head to focus on a particular aspect such as entity grounding or relational chaining. Unlike MRAG (Besta et al., 2024), which treats heads as independent embedding channels, our symmetric decomposition enforces structural alignment between the two sides, enabling coherent and complementary semantic spaces.

3.2 Balancing Exploration and Exploitation

Creating multiple semantic views introduces flexibility but also tension: the model must encourage heads to explore distinct reasoning cues, yet prevent them from drifting toward irrelevant or redundant information. ParallaxRAG balances them through *exploration* for head diversity and *exploitation* for query relevance.

Exploration: Pairwise Similarity Regulation. During structural propagation at layer ℓ , each head k performs message passing to integrate neighborhood context:

$$\tilde{H}_k^{(\ell+1)}(v_i) = \sum_{v_j \in \mathcal{N}(v_i)} \frac{1}{|\mathcal{N}(v_i)|} H_k^{(\ell)}(v_j) W^{(\ell)}.$$

While this process spreads information across entities, multiple heads could converge to similar activation patterns. To maintain diversity, PSR measures the overlap among heads via their activation summaries:

$$\mathbf{s}_k^{(\ell)} = \frac{\tilde{H}_k^{(\ell+1)} \mathbf{1}_d}{\|\tilde{H}_k^{(\ell+1)} \mathbf{1}_d\|_2}, \quad r_k^{(\ell)} = \sum_{j \neq k} \langle \mathbf{s}_k^{(\ell)}, \mathbf{s}_j^{(\ell)} \rangle.$$

Each head’s update is then adaptively scaled by a diversity coefficient:

$$H_k^{(\ell+1)} = e^{-\beta r_k^{(\ell)}} \tilde{H}_k^{(\ell+1)},$$

where β controls the penalty strength. This keeps the retrieval process exploratory—heads remain distinct, each probing a different facet of the graph.

Exploitation: Query-Aware Gating with Weak Supervision. To focus retrieval on the most relevant heads for a given question, a lightweight gate maps the global query embedding \mathbf{q} (final [CLS] token) to head-importance weights

$$\boldsymbol{\alpha} = \text{softmax}(W_g \mathbf{q}) \in \mathbb{R}^H.$$

Each head’s shared MLP scores candidate triples, yielding $Z \in \mathbb{R}^{|E| \times H}$; gated aggregation produces

$$\mathbf{s} = Z\boldsymbol{\alpha}, \quad P_{\text{pred}} = \text{softmax}(\mathbf{s}).$$

For each question, we extract the shortest paths linking its topic and answer entities in the KG. Triples on these paths (\mathcal{T}_{sp}) form the weak supervision signal, defining a normalized target distribution:

$$P_{\text{true}}(\tau) = \frac{\mathbb{I}[\tau \in \mathcal{T}_{\text{sp}}] w_\tau}{\sum_{\tau' \in \mathcal{E}} \mathbb{I}[\tau' \in \mathcal{T}_{\text{sp}}] w_{\tau'}}.$$

The retriever is trained end-to-end by minimizing

$$\mathcal{L} = \text{KL}(P_{\text{true}} \| P_{\text{pred}}),$$

which guides the gate and heads to emphasize triples composing the shortest topic–answer reasoning chains.

3.3 Grounded Reasoning with LLMs

The top- k retrieved triples are linearized and concatenated with the question, together with a one-shot demonstration, to construct an evidence-grounded prompt for the LLM. This prompt formulation provides explicit relational context for each reasoning step and ensures that the model’s generation remains aligned with hop-specific evidence derived from the multi-view retriever.

4 Experiments

We design a series of experiments to examine whether multi-view decoupling leads to more reliable and interpretable multi-hop reasoning. Specifically, we investigate three key questions: **RQ1**:

Does ParallaxRAG retrieve cleaner and more relevant subgraphs efficiently? **RQ2**: Do multi-head views specialize in different reasoning stages and improve retrieval quality? **RQ3**: Can ParallaxRAG enhance answer grounding and reduce hallucination in end-to-end KGQA? Sections 4.2, 4.4 and 4.5 address RQ1, Section 4.3 analyzes RQ2, and Section 4.4 further studies RQ3.

4.1 Experiment Setup

Datasets. We use WebQSP and CWQ benchmark and further test cross-domain generalization on BioASQ, which requires biomedical factual reasoning.

Baselines.

Retrieval Baselines. We compare against representative retrieval paradigms: structure-free (Cosine Similarity (Li et al., 2024)), path-based (SR+NSM (Zhang et al., 2022), Retrieve-Rewrite-Answer (Wu et al., 2023), RoG (Luo et al., 2023)), hybrid (G-Retriever (He et al., 2024)), and GNN-based (GNN-RAG (Mavromatis and Karypis, 2024)).

End-to-End KGQA Baselines. We further evaluate against state-of-the-art KGQA models—UniKGQA (Jiang et al., 2022), KD-CoT (Zhao et al., 2024), StructGPT (Jiang et al., 2023), ToG (Sun et al., 2023), and EtD (Liu et al., 2024). Following (Zhang et al., 2022), we adopt the RoG-Sep variant to avoid label leakage in RoG-Joint training.

Implementation Details. All retrievers use the BGE-M3¹ encoder for consistency. Baselines are reproduced from official implementations. Key hyperparameters and training details are listed in Appendix B. Results using alternative backbones are shown in Appendix C.3.

Metrics. We report both retrieval and end-to-end performance. *Retrieval*: (i) shortest-path triple recall, (ii) GPT-4o-verified triple recall, and (iii) answer-entity recall, averaged per query and broken down by hop length. *Efficiency*: wall-clock inference time on an RTX 6000 Ada GPU (excluding KG I/O). *End-to-end QA*: Macro-F1 and Hit scores on WebQSP/CWQ, plus domain metrics on BioASQ.

¹<https://huggingface.co/BAAI/bge-m3>

Table 1: Main retrieval recall evaluation results for different models on WebQSP and CWQ datasets.

Model	Shortest Path Triple Recall						GPT-4o Triple Recall						Answer Entity Recall					
	WebQSP			CWQ			WebQSP			CWQ			WebQSP			CWQ		
	1 (65.8%)	2 (34.2%)	1 (28.0%)	2 (65.9%)	≥ 3 (6.1%)	1 (65.8%)	2 (34.2%)	1 (28.0%)	2 (65.9%)	≥ 3 (6.1%)	1 (65.8%)	2 (34.2%)	1 (28.0%)	2 (65.9%)	≥ 3 (6.1%)	1 (65.8%)	2 (34.2%)	≥ 3 (6.1%)
cosine similarity	0.874	0.405	0.629	0.442	0.333	0.847	0.483	0.629	0.511	0.464	0.943	0.253	0.903	0.472	0.289			
SR+NSM w E2E	0.565	0.324	-	-	-	0.580	0.376	-	-	-	0.916	0.301	-	-	-			
Retrieve-Rewrite-Answer	0.064	0.046	-	-	-	0.062	0.061	-	-	-	0.745	0.729	-	-	-			
RoG	0.869	0.415	0.766	0.597	0.253	0.446	0.271	0.347	0.293	0.122	0.874	0.677	0.920	0.827	0.628			
G-Retriever	0.335	0.216	0.134	0.205	0.168	0.345	0.284	0.159	0.240	0.226	0.596	0.446	0.377	0.384	0.269			
GNN-RAG	0.532	0.502	0.515	0.498	0.446	0.384	0.445	0.328	0.408	0.418	0.810	0.831	0.853	0.841	0.787			
SubgraphRAG	0.954	0.720	0.845	0.826	0.609	0.895	0.768	0.787	0.810	0.725	0.979	0.844	0.937	0.918	0.683			
ParallaxRAG	0.966	0.761	0.916	0.818	0.578	0.923	0.825	0.847	0.845	0.760	0.986	0.899	0.962	0.935	0.771			

4.2 Retrieval Performance (RQ1)

Table 1 summarizes the retrieval results. ParallaxRAG consistently delivers strong performance across all datasets and metrics, with advantages that become more evident as the reasoning depth increases. On WebQSP, it achieves 0.986 and 0.899 in 1-hop and 2-hop entity recall, surpassing all baselines. On the more challenging CWQ dataset, it maintains robust retrieval up to 3-hop questions, reaching 0.935 in 2-hop and 0.771 in ≥ 3 -hop Answer Entity Recall—an 12.9% improvement over SubgraphRAG. These results indicate that ParallaxRAG is particularly effective in handling complex reasoning chains where the retrieval space grows noisy and combinatorial.

In terms of efficiency, ParallaxRAG remains computationally lightweight, requiring 40 seconds on WebQSP and 84 seconds on CWQ (excluding KG I/O), compared to 948 and 2327 seconds for RoG, 672 and 1530 seconds for G-Retriever. This demonstrates that multi-view reasoning can enhance precision and robustness without incurring significant computational cost. Overall, ParallaxRAG retrieves more answer-relevant subgraphs, validating the effectiveness of its exploration-exploitation design.

4.3 Attention Head Specialization (RQ2)

Figure 3 reveals a clear division of labor among ParallaxRAG’s attention heads that adapts to query complexity. For short-hop questions in WebQSP, early heads dominate, focusing on direct entity associations. As the reasoning chain extends in CWQ, later heads become increasingly active, capturing relational dependencies across multiple hops. This dynamic shift forms a relay pattern, where information is progressively passed from surface-level to abstract semantic heads as reasoning deepens.

We quantify this specialization by training a lin-

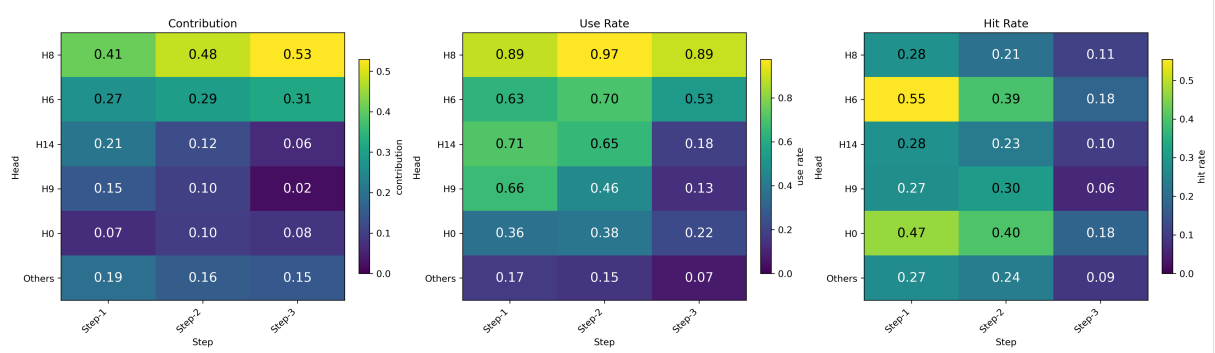
Table 2: Question-answering performance on WebQSP and CWQ. The Hallucination (Hallu.) score is evaluated on a subset that excludes samples where the answer entity is not in the KG, following (Li et al., 2024). Our generators use the top 100 retrieved triples by default; results for 200 and 500 (indicated in parentheses) are also shown. Best results are in **bold**. Results with (\leftrightarrow) evaluate retriever generalizability, where the retriever is trained on one dataset and applied to the other.

Model	WebQSP			CWQ		
	Macro-F1	Hit	Hallu.	Macro-F1	Hit	Hallu.
<i>(A) Neural Methods</i>						
UniKQQA	72.2	-	-	49.0	-	-
SR+NSM w E2E	64.1	-	64.44	46.3	-	-
<i>(B) Multi-turn LLM Reasoning Methods</i>						
KD-CoT	52.5	68.6	-	-	55.7	-
ToG (GPT-4)	-	82.6	-	-	67.6	-
StructGPT	-	74.69	-	-	-	-
Retrieve-Rewrite-Answer	-	79.36	-	-	-	-
RoG-Joint	70.26	86.67	76.13	54.63	61.94	55.15
RoG-Sep	66.45	82.19	72.79	53.87	60.55	54.51
<i>(C) RAG-based Methods</i>						
G-Retriever	53.41	73.46	67.97	-	-	-
EID	-	82.5	-	-	62.0	-
GNN-RAG	71.3	85.7	-	59.4	66.8	-
SubgraphRAG	76.46	89.80	81.85	59.08	66.69	66.57
ParallaxRAG + Llama3.1-8B	71.73	86.85	83.64	48.33	58.41	66.12
ParallaxRAG + Qwen3-30B	75.24	91.60	75.45	59.25	65.30	57.18
ParallaxRAG + Qwen3-30B (200)	76.07	92.48	76.23	59.31	66.21	58.06
ParallaxRAG + Qwen3-30B (500)	76.11	93.26	77.86	59.18	64.52	60.07
ParallaxRAG + GPT-4o (200)	77.82	93.63	82.94	61.22	67.72	66.69
<i>(D) Cross-dataset Generalization (\leftrightarrow)</i>						
SubgraphRAG + Llama3.1-8B (\leftrightarrow)	66.42	83.42	80.09	37.96	48.57	56.78
ParallaxRAG + Llama3.1-8B (\leftrightarrow)	69.22	89.51	82.64	45.28	54.82	60.04

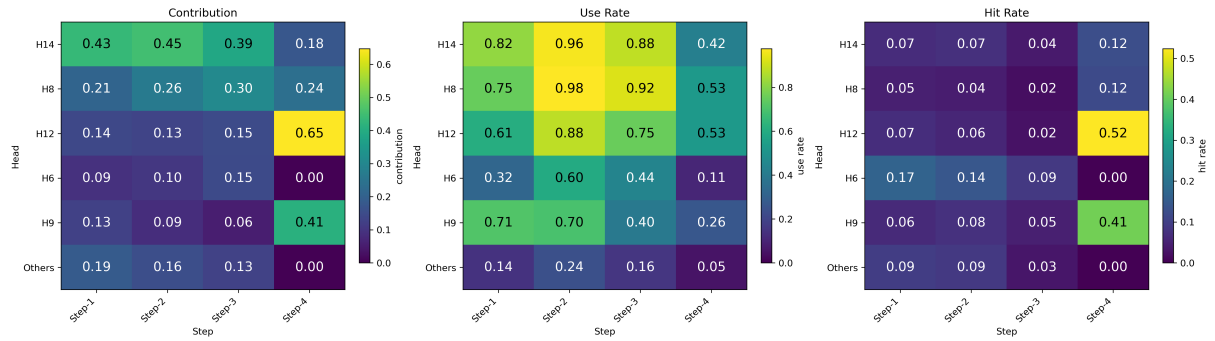
ear probe to predict reasoning depth from head activations, achieving 46.5% accuracy compared to a 25% random baseline, demonstrating that head activations encode distinct reasoning stages. To establish causality, we perform a Difference-in-Differences-in-Differences (DDD) analysis comparing performance drops after ablating specialist versus random heads across short and long queries:

$$\text{DDD} = [(\Delta_{\text{Long}}^{\text{Specialist}} - \Delta_{\text{Short}}^{\text{Specialist}})] - [(\Delta_{\text{Long}}^{\text{Random}} - \Delta_{\text{Short}}^{\text{Random}})]$$

where Δ denotes the post-ablation performance difference. A significant negative DDD value of -0.0184 (95% CI: [-0.0248, -0.0045], $p=0.0055$) confirms that specialist heads are functionally non-substitutable, playing distinct roles essential for



(a) WebQSP: Early-Step Specialization for Short-Chain Reasoning



(b) CWQ: Dynamic Head Specialization Switching for Long-Chain Reasoning

Figure 3: Visualization of attention head specialization, revealing a task-adaptive division of labor. The heatmaps display three metrics (Contribution, Use Rate, Hit Rate) for the top 5 specialist heads, selected from our BGE-based model’s 16 heads according to their overall contribution. The Others row aggregates the remaining 11 heads: for Contribution, this value is the sum of their contributions, while for Use Rate and Hit Rate, it is their average, see more explanation in (Appendix C). We define *steps* as the BFS expansion depth along reasoning paths, rather than the conventional hop (shortest-path length), in order to capture head behaviors at each layer of candidate exploration. **(a)** On WebQSP (short chains). **(b)** On CWQ (long chains).

multi-hop reasoning.

Together, these findings demonstrate that dynamic head specialization is not a byproduct of training noise, but an emergent coordination mechanism that enables efficient multi-hop reasoning across diverse question types.

4.4 End-to-End KGQA with RAG (RQ1 & RQ3)

We next examine whether the retrieval and head-specialization advantages of ParallaxRAG lead to improvements in downstream question answering. As shown in Table 2, when paired with Llama3.1-8B and using 100 retrieved triples, ParallaxRAG attains a Macro-F1 of 71.73 and a Hit rate of 86.85 on WebQSP, and delivers comparable performance on CWQ. When combined with GPT-4o and an expanded context of 200 triples, the model establishes new state-of-the-art results, reaching a Macro-F1 of 77.82 and a Hit rate of 93.63 on WebQSP, while also achieving 61.22 Macro-F1 and 67.72 Hit on

CWQ.

Beyond overall accuracy, ParallaxRAG improves reliability by reducing hallucinated generations. On hallucination-controlled subsets (Li et al., 2024), hallucination scores decrease by 1.22% on WebQSP and 3.23% on CWQ, indicating that the retrieved subgraphs are not only sufficient but also cleaner and more grounded. Qualitative examples in Appendix D further illustrate this effect: for long-chain CWQ questions, ParallaxRAG retrieves fewer but more relevant triples, enabling coherent reasoning chains that accurately support the final answers.

4.5 Domain Generalization (RQ1)

To evaluate cross-domain robustness, we test ParallaxRAG on the biomedical BioASQ benchmark (Task B), which includes Yes/No, Factoid, and List questions. Following the same retrieval pipeline, where the retriever is trained on CWQ, we use Qwen3-Plus as generator and report official met-

Model	Yes/No Questions				Factoid Questions			List Questions		
	Acc.	F1 Yes	F1 No	Macro F1	Strict	Lenient	MRR	Prec.	Recall	F1
Deepseek-R1-8B	0.9077	0.9312	0.8558	0.8935	0.2620	0.2733	0.2677	0.3982	0.3427	0.3517
GPT4-Turbo	0.9129	0.9357	0.8616	0.8986	0.5505	0.6515	0.6010	0.5788	0.4857	0.5051
GPT-4o	0.9140	0.9347	0.8670	0.9009	0.3462	0.3462	0.3462	0.5102	0.4025	0.4330
ParallaxRAG + Qwen3-Plus	0.9351	0.9524	0.8980	0.9252	0.4210	0.8222	0.8667	0.7116	0.4569	0.4737

Table 3: Generalization on BioASQ benchmark and comparison among our baseline and general LLM, Our baseline shows impressive effect on Lenient Accuracy and MRR on Factoid questions

Table 4: Ablation study on WebQSP and CWQ, analyzing the impact of ParallaxRAG’s core multi-head architecture and its synergistic mechanisms. Values in parentheses (↓) indicate the performance drop compared to the full model (Llama3.1-8B as generator).

Configuration	WebQSP		CWQ	
	Macro-F1	Hit	Macro-F1	Hit
ParallaxRAG (Full Model)	71.73	86.85	48.33	58.41
Multi-Head Architecture Validation				
(a) Split Vector Baseline	69.42 (↓2.31)	85.02 (↓1.83)	42.27 (↓6.06)	51.54 (↓6.87)
(b) Single Vector Baseline	70.60 (↓1.13)	86.11 (↓0.74)	44.82 (↓3.51)	52.63 (↓5.78)
Synergistic Mechanism Validation				
(c) Without PSR	69.73 (↓0.73)	85.47 (↓0.35)	47.12 (↓1.21)	56.32 (↓2.09)
(d) Without Query-Aware Gating	56.25 (↓15.48)	74.69 (↓12.16)	29.14 (↓19.19)	38.26 (↓20.15)

rics: accuracy and F1 for Yes/No, strict and lenient accuracy with MRR for Factoid, and precision, recall, and F1 for List questions.

Table 3 shows that ParallaxRAG achieves the best Yes/No results (accuracy 0.9351, F1 0.9252), outperforming strong general-purpose LLMs. On Factoid questions, it attains a lenient accuracy of 0.8222 and an MRR of 0.8667, reflecting effective multi-view reasoning even under domain shift. For List questions, ParallaxRAG favors precision (0.7116) over recall (0.4569), resulting in a slightly lower F1 than GPT-4-Turbo (0.4737 vs. 0.5051), suggesting a bias toward concise, high-confidence retrieval.

Overall, these results demonstrate that ParallaxRAG generalizes well to specialized biomedical domains without retriever retraining, maintaining strong grounding on binary and factoid queries while remaining competitive on open-ended list reasoning.

4.6 Ablation Study

We conducted an ablation study on WebQSP and CWQ to examine the contributions of ParallaxRAG’s core architecture and its synergistic components. Table 4 summarizes the results.

First, to verify the role of the multi-head design, we compare two simplified baselines. The Split

Vector variant divides a single query embedding into pseudo-heads without true head specialization, causing a Macro-F1 drop of 2.31 on WebQSP and 6.06 on CWQ. Similarly, the Single Vector variant—using a flat embedding—shows performance drops of 1.13 and 3.51 points, confirming that learned multi-head representations are crucial for capturing distinct relational cues and mitigating representational collapse.

Next, we evaluate the synergistic mechanisms. Removing Pairwise Similarity Regularization (PSR) yields redundant head behavior and reduces Macro-F1 by 0.73 and 1.21 points, demonstrating PSR’s role in maintaining head diversity. Eliminating the query-aware gating and replacing it with simple averaging leads to severe performance degradation, with Hit rate drops of 12.16 and 20.15 points, underscoring its necessity for dynamic head weighting and precise retrieval.

Overall, these findings highlight that ParallaxRAG’s strength lies in the interaction between its multi-view architecture and the exploration-exploitation balance enforced by PSR and adaptive gating. Ablating any of these components increases subgraph noise and weakens reasoning stability, reaffirming the importance of the framework’s holistic design.

5 Limitations and Future Work

While ParallaxRAG demonstrates strong retrieval performance and effectively captures head-level specialization, we identify several limitations that suggest directions for future work.

First, our method relies on the quality of the underlying knowledge graph and embedding model; errors in these components may propagate to retrieval performance. In addition, the current implementation focuses on static knowledge graphs and does not address dynamic or continuously updated settings. We leave extensions to noisier and larger-scale knowledge sources as future work.

Second, as observed in our case study, the multi-view mechanism can be over-expressive for shallow queries (e.g., 1-hop transitive relations). By surfacing diverse but weakly relevant constraints, the retriever may introduce additional noise, which can reduce the effectiveness of downstream LLM reasoning and lead to conservative answer behavior. Future work could explore adaptive or agentic mechanisms that dynamically adjust retrieval complexity based on query difficulty.

References

Akari Asai, Zequi Wu, Yizhong Wang, Avirup Sil, and Hannaneh Hajishirzi. 2024. Self-rag: Learning to retrieve, generate, and critique through self-reflection.

Maciej Besta, Ales Kubicek, Robert Gerstenberger, Marcin Chrapek, Roman Niggli, Patrik Okanovic, Yi Zhu, Patrick Iff, Michal Podstawska, Lucas Weitzendorf, and 1 others. 2024. Multi-head rag: Solving multi-aspect problems with llms. *arXiv preprint arXiv:2406.05085*.

Srinadh Bhojanapalli, Ayan Chakrabarti, Andreas Veit, Michal Lukasik, Himanshu Jain, Frederick Liu, Yin-Wen Chang, and Sanjiv Kumar. 2021. Leveraging redundancy in attention with reuse transformers. *arXiv preprint arXiv:2110.06821*.

Yuchen Bian, Jiaji Huang, Xingyu Cai, Jiahong Yuan, and Kenneth Church. 2021. On attention redundancy: A comprehensive study. In *Proceedings of the 2021 conference of the north american chapter of the association for computational linguistics: human language technologies*, pages 930–945.

Bin Fu, Yunqi Qiu, Chengguang Tang, Yang Li, Haiyang Yu, and Jian Sun. 2020. A survey on complex question answering over knowledge base: Recent advances and challenges. *arXiv preprint arXiv:2007.13069*.

Ruiliu Fu, Han Wang, Xuejun Zhang, Jun Zhou, and Yonghong Yan. 2021. Decomposing complex questions makes multi-hop qa easier and more interpretable. *arXiv preprint arXiv:2110.13472*.

Yunfan Gao, Yun Xiong, Xinyu Gao, Kangxiang Jia, Jinliu Pan, Yuxi Bi, Yixin Dai, Jiawei Sun, Haofen Wang, and Haofen Wang. 2023. Retrieval-augmented generation for large language models: A survey. *arXiv preprint arXiv:2312.10997*, 2(1).

Xiaoxin He, Yijun Tian, Yifei Sun, Nitesh Chawla, Thomas Laurent, Yann LeCun, Xavier Bresson, and Bryan Hooi. 2024. G-retriever: Retrieval-augmented generation for textual graph understanding and question answering. *Advances in Neural Information Processing Systems*, 37:132876–132907.

Gautier Izacard and Edouard Grave. 2020. Leveraging passage retrieval with generative models for open domain question answering. *arXiv preprint arXiv:2007.01282*.

Gautier Izacard, Patrick Lewis, Maria Lomeli, Lucas Hosseini, Fabio Petroni, Timo Schick, Jane Dwivedi-Yu, Armand Joulin, Sebastian Riedel, and Edouard Grave. 2022. Few-shot learning with retrieval augmented language models. *arXiv preprint arXiv:2208.03299*, 1(2):4.

Shaoxiong Ji, Shirui Pan, Erik Cambria, Pekka Marttinen, and Philip S Yu. 2021. A survey on knowledge graphs: Representation, acquisition, and applications. *IEEE transactions on neural networks and learning systems*, 33(2):494–514.

Jinhao Jiang, Kun Zhou, Zican Dong, Keming Ye, Wayne Xin Zhao, and Ji-Rong Wen. 2023. Structgpt: A general framework for large language model to reason over structured data. *arXiv preprint arXiv:2305.09645*.

Jinhao Jiang, Kun Zhou, Wayne Xin Zhao, and Ji-Rong Wen. 2022. Unikgqa: Unified retrieval and reasoning for solving multi-hop question answering over knowledge graph. *arXiv preprint arXiv:2212.00959*.

Vladimir Karpukhin, Barlas Oguz, Sewon Min, Patrick SH Lewis, Ledell Wu, Sergey Edunov, Danqi Chen, and Wen-tau Yih. 2020. Dense passage retrieval for open-domain question answering. In *EMNLP (1)*, pages 6769–6781.

Omar Khattab and Matei Zaharia. 2020. Colbert: Efficient and effective passage search via contextualized late interaction over bert. In *Proceedings of the 43rd International ACM SIGIR conference on research and development in Information Retrieval*, pages 39–48.

Patrick Lewis, Ethan Perez, Aleksandra Piktus, Fabio Petroni, Vladimir Karpukhin, Naman Goyal, Heinrich Kütter, Mike Lewis, Wen-tau Yih, Tim Rocktäschel, and 1 others. 2020. Retrieval-augmented generation for knowledge-intensive nlp tasks. *Advances in neural information processing systems*, 33:9459–9474.

Mufei Li, Siqi Miao, and Pan Li. 2024. Simple is effective: The roles of graphs and large language models in knowledge-graph-based retrieval-augmented generation. *arXiv preprint arXiv:2410.20724*.

Tsung-Yi Lin, Priya Goyal, Ross Girshick, Kaiming He, and Piotr Dollár. 2017. Focal loss for dense object detection. In *Proceedings of the IEEE International Conference on Computer Vision (ICCV)*, pages 2980–2988.

Guangyi Liu, Yongqi Zhang, Yong Li, and Quanming Yao. 2024. Explore then determine: A gnn-llm synergy framework for reasoning over knowledge graph. *arXiv e-prints*, pages arXiv–2406.

Nelson F Liu, Kevin Lin, John Hewitt, Ashwin Paranjape, Michele Bevilacqua, Fabio Petroni, and Percy Liang. 2023. Lost in the middle: How language models use long contexts. *arXiv preprint arXiv:2307.03172*.

Linhao Luo, Yuan-Fang Li, Gholamreza Haffari, and Shirui Pan. 2023. Reasoning on graphs: Faithful and interpretable large language model reasoning. *arXiv preprint arXiv:2310.01061*.

Costas Mavromatis and George Karypis. 2024. Gnn-rag: Graph neural retrieval for large language model reasoning. *arXiv preprint arXiv:2405.20139*.

Geondo Park, Chihye Han, Wonjun Yoon, and Daeshik Kim. 2020. Mhsan: Multi-head self-attention network for visual semantic embedding. In *Proceedings*

of the IEEE/CVF winter conference on applications of computer vision, pages 1518–1526.

Boci Peng, Yun Zhu, Yongchao Liu, Xiaohe Bo, Haizhou Shi, Chuntao Hong, Yan Zhang, and Siliang Tang. 2024. Graph retrieval-augmented generation: A survey. *arXiv preprint arXiv:2408.08921*.

Ethan Perez, Patrick Lewis, Wen-tau Yih, Kyunghyun Cho, and Douwe Kiela. 2020. Unsupervised question decomposition for question answering. *arXiv preprint arXiv:2002.09758*.

Fabio Petroni, Aleksandra Piktus, Angela Fan, Patrick Lewis, Majid Yazdani, Nicola De Cao, James Thorne, Yacine Jernite, Vladimir Karpukhin, Jean Maillard, and 1 others. 2020. Kilt: a benchmark for knowledge intensive language tasks. *arXiv preprint arXiv:2009.02252*.

Jiashuo Sun, Chengjin Xu, Lumingyuan Tang, Saizhuo Wang, Chen Lin, Yeyun Gong, Lionel M Ni, Heung-Yeung Shum, and Jian Guo. 2023. Think-on-graph: Deep and responsible reasoning of large language model on knowledge graph. *arXiv preprint arXiv:2307.07697*.

Harsh Trivedi, Niranjan Balasubramanian, Tushar Khot, and Ashish Sabharwal. 2022. Interleaving retrieval with chain-of-thought reasoning for knowledge-intensive multi-step questions. *arXiv preprint arXiv:2212.10509*.

Varun Vashisht, Samar Singh, Mihir Konduskar, Jaskaran Singh Walia, and Vukosi Marivate. 2025. Mage: Multi-head attention guided embeddings for low resource sentiment classification. *arXiv preprint arXiv:2502.17987*.

Ashish Vaswani, Noam Shazeer, Niki Parmar, Jakob Uszkoreit, Llion Jones, Aidan N Gomez, Łukasz Kaiser, and Illia Polosukhin. 2017. Attention is all you need. *Advances in neural information processing systems*, 30.

Jason Wei, Xuezhi Wang, Dale Schuurmans, Maarten Bosma, Fei Xia, Ed Chi, Quoc V Le, Denny Zhou, and 1 others. 2022. Chain-of-thought prompting elicits reasoning in large language models. *Advances in neural information processing systems*, 35:24824–24837.

Yike Wu, Nan Hu, Sheng Bi, Guilin Qi, Jie Ren, An-huan Xie, and Wei Song. 2023. Retrieve-rewrite-answer: A kg-to-text enhanced llms framework for knowledge graph question answering. *arXiv preprint arXiv:2309.11206*.

Jing Zhang, Xiaokang Zhang, Jifan Yu, Jian Tang, Jie Tang, Cuiping Li, and Hong Chen. 2022. Subgraph retrieval enhanced model for multi-hop knowledge base question answering. In *Proceedings of the 60th Annual Meeting of the Association for Computational Linguistics (Volume 1: Long Papers)*, pages 5773–5784.

Ruilin Zhao, Feng Zhao, Long Wang, Xianzhi Wang, and Guandong Xu. 2024. Kg-cot: Chain-of-thought prompting of large language models over knowledge graphs for knowledge-aware question answering. In *Proceedings of the Thirty-Third International Joint Conference on Artificial Intelligence (IJCAI-24)*, pages 6642–6650. International Joint Conferences on Artificial Intelligence.

A Implementation Details of the ParallaxRAG Framework

A.1 Detailed Derivation of Pairwise Similarity Regulation (PSR)

The Pairwise Similarity Regulation (PSR) mechanism is integrated into each layer of the Distance Encoding (DE) to foster representational diversity.

1. DE Propagation. Given the initial one-hot topic entity features $\mathbf{X}_0 \in \mathbb{R}^{N \times 2}$, the model performs L_f forward and L_r reverse propagation layers. Each layer ℓ computes a preliminary update $\tilde{\mathbf{H}}_k^{(\ell+1)}$ for each head k via message passing (MP):

$$\tilde{\mathbf{H}}_k^{(\ell+1)} = \text{MP}(\mathbf{E}, \mathbf{H}_k^{(\ell)}) \quad (\text{forward pass, using edge index } \mathbf{E})$$

The reverse pass is analogous, using the transposed edge index \mathbf{E}^T .

2. PSR Computation and Application. After each propagation step, the preliminary updates $\tilde{\mathbf{H}}$ are modulated by PSR. The process begins by computing a node intensity vector $\mathbf{s}_k^{(\ell)}$ for each head to capture its activation distribution:

$$\mathbf{s}_k^{(\ell)} = \text{L2Norm} \left(\sum_d \tilde{\mathbf{H}}_k^{(\ell)}[:, d] \right)$$

These vectors are then used to derive a redundancy score $r_k^{(\ell)}$ from pairwise similarities, which in turn defines the regulation coefficient $\alpha_k^{(\ell)}$:

$$r_k^{(\ell)} = \sum_{j \neq k} \langle \mathbf{s}_i^{(\ell)}, \mathbf{s}_j^{(\ell)} \rangle \quad \Rightarrow \quad \alpha_k^{(\ell)} = \exp(-\beta \cdot r_k^{(\ell)})$$

Finally, this coefficient performs the final update by scaling the preliminary update to produce the final layer output:

$$\mathbf{H}_k^{(\ell+1)} = \alpha_k^{(\ell)} \cdot \tilde{\mathbf{H}}_k^{(\ell+1)}$$

3. Final Representation. The final structural representations \mathcal{H}_k for each head are formed by collecting the outputs $\{\mathbf{H}_k^{(\ell)}\}$ from all layers, which are then used for triple scoring.

A.2 Weighted Listwise Training Objective

To handle the severe class imbalance in retrieval, we convert the binary weak supervision signal $\mathbf{y} \in \{0, 1\}^{|\mathcal{E}|}$ into a weighted target distribution for our listwise objective.

1. Positive Reweighting. The binary vector \mathbf{y} is first normalized. Then, a weight factor w_τ is applied to construct the final weighted distribution. In our implementation, we use $w_\tau = 10$ for positive triples ($y_\tau = 1$) and $w_\tau = 1$ otherwise. This is conceptually similar to the α -balancing in Focal Loss (Lin et al., 2017).

$$y_\tau^{\text{norm}} = \frac{y_\tau}{\sum_{\tau'} y_{\tau'}}, \quad y_\tau^{\text{weighted}} = \frac{y_\tau \cdot w_\tau}{\sum_{\tau'} (y_{\tau'} \cdot w_{\tau'})}$$

2. Final Loss Formulation. The model is trained by minimizing the weighted listwise cross-entropy (equivalent to KL divergence) between the predicted distribution P_{pred} and the target y^{weighted} :

$$\mathcal{L}_{\text{listwise}} = - \sum_{\tau \in \mathcal{E}} y_\tau^{\text{weighted}} \log (P_{\text{pred}}(\tau) + \epsilon)$$

B Additional Experiment Setting

B.1 Implementation Details for ParallaxRAG

Our model is implemented in PyTorch and PyTorch Geometric. The ParallaxRAG retriever, which consists of a BGE-M3 text encoder, a PSR-enhanced DE module, and a scoring MLP, is trained end-to-end for up to 100 epochs with an early stopping patience of 20. The forward and reverse propagation round is set to 2 rounds, with PSR strength of 0.5. We use the AdamW optimizer with a half-cycle cosine annealing with warmup learning rate, during a warmup phase for the first few epochs, the learning rate linearly increases from 0 to a peak value of 1×10^{-3} . Following the warmup, the learning rate is smoothly decayed along a cosine curve to a minimum value of 1×10^{-5} . to enable finer parameter adjustments in the later stages of training. an effective batch size of 2 (via gradient accumulation), and employ a weighted listwise ranking loss.

For the end-to-end KGQA task, the top-100 triples retrieved are linearized into a natural text format and prepended to the question as context for a LLM generator. We generate final answers using nucleus sampling with $p = 0.95$ and a temperature of 0.7.

To ensure a fair comparison, all baseline models follow the experimental setup from Zhang et al.

(2022). our pipeline as well as the newest baseline Subgraph RAG use BGE-M3 as backbone text encoder.

B.2 Prompt Templates

Figure 6 is the detailed prompt template used in our experiments for all samples.

B.3 Hyperparameter Sensitivity Analysis

In this section, we analyze the sensitivity of our model to the key hyperparameter β , which controls the strength of the Pairwise Similarity Regulation (PSR). We argue that a challenging zero-shot transfer task is the most effective setting to demonstrate PSR’s true diversity impact, as it enables the model to maximally leverage its learned head specialization. Therefore, we evaluate a model trained on WebQSP on the CWQ test set, varying β within the range of $\{0.2, 0.5, 2.0\}$, with $\beta = 0$ serving as the baseline without diversity regulation.

As shown in Figure 4, the results under this stringent evaluation setting are revealing. A moderate PSR strength of $\beta = 0.5$ achieves the peak performance, boosting the Macro-F1 from a baseline of 50.54 to 50.93 and the Hit rate from 61.87 to 62.51. This performance gain suggests that the diverse representations fostered by PSR are indeed learning more generalizable reasoning mechanisms. The degradation at a high penalty ($\beta = 2.0$) indicates the limit of this effect, where excessive suppression can hinder signal propagation. These findings not only validate our choice of $\beta = 0.5$ for the main experiments but also underscore that the generalization task is a fitting benchmark to reveal the true benefits of the PSR mechanism.

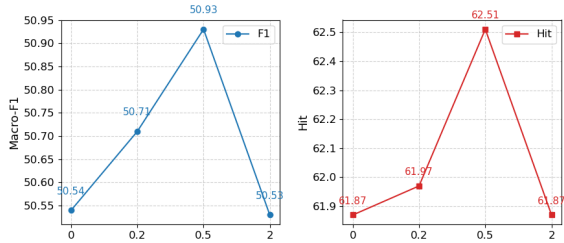


Figure 4: Sensitivity analysis of the PSR strength parameter β on the generalization task, where the retriever was trained on WebQSP and tested on CWQ, using Llama-3.1-8B as the generator.

C Attention Head Analysis Details

This section provides the detailed methodology for the attention head analysis presented in Section 4.3.

We formally define the concepts of reasoning *steps* and the three metrics used to evaluate head-level performance.

C.1 Defining Reasoning Steps

To formally quantify head performance during multi-hop reasoning, we define *steps* as the Breadth-First Search (BFS) expansion depth along reasoning paths. This is distinct from the conventional definition of a *hop* (i.e., the final shortest-path length) and allows us to capture head behaviors at each layer of candidate exploration. For example, if the topic entity is “Barack Obama,” Step-1 includes triples directly connected to him, such as (Obama, born_in, Honolulu). Step-2 then expands from the entities retrieved in Step-1, considering candidates like (Honolulu, located_in, Hawaii).

C.2 Head Performance Metrics

We define three complementary metrics to evaluate the role and effectiveness of each attention head during the reasoning process.

Contribution Measures a head’s share of credit for retrieving correct triples at a given step. It is defined as the proportion of correctly retrieved triples for which this head provided the highest score.

$$\text{Contribution}(h, t) = \frac{|C(h, t) \cap A_t \cap G_t|}{|A_t \cap G_t|}$$

Use Rate Measures the model’s overall reliance on a head. It is the proportion of samples where a triple scored highest by head h was ultimately selected by the model’s gating mechanism at step t .

$$\text{Use Rate}(h, t) = \frac{|\mathcal{S}(h, t)|}{|\mathcal{S}_t|}$$

Hit Rate Measures the precision of a head’s top-scoring suggestions. It is the percentage of a head’s suggestions selected by the gate that are actually correct.

$$\text{Hit Rate}(h, t) = \frac{|C(h, t) \cap A_t \cap G_t|}{|C(h, t) \cap A_t|}$$

where, for any given head h and reasoning step t , G_t is the set of ground-truth triples, and A_t is the set of triples actually retrieved by the gated model. The term $C(h, t)$ represents the set of candidate

triples for which head h provided the highest score among all heads. Finally, \mathcal{S}_t is the set of all samples that require reasoning at step t , while $\mathcal{S}(h, t)$ is the subset of those samples where a triple from $C(h, t)$ was selected by the final gating mechanism.

C.3 Head Specialization with Alternative Backbone Encoders

To confirm the generalizability of the head specialization phenomenon, we tested the ParallaxRAG framework using two alternative, high-performance backbone encoders: intfloat/e5-large-v2 and thenlper/gte-large. Our analysis confirms that the core phenomenon of head specialization persists across all tested encoders, though the specific cooperative patterns among heads vary, reflecting different emergent strategies for multi-hop reasoning.

C.3.1 intfloat/e5-large-v2 Analysis (Figure 5a)

The e5-large-v2 encoder consistently validates the functional division of labor. Head 10 (Contribution: 0.60, Use Rate: 0.96) and Head 2 (Contribution: 0.52, Use Rate: 0.94) emerged as the dominant initial-step specialists (peaking at Step-1 for entity localization). Conversely, Head 3 demonstrated the highest precision for terminal reasoning, achieving a Hit Rate of 0.50 at Step-4. This confirms the learned segregation between high-activation front-end heads and high-precision terminal heads. However, the magnitude of the dynamic switching effect was marginally less pronounced compared to BGE-M3, suggesting a more continuous contribution profile.

C.3.2 thenlper/gte-large Analysis (Figure 5b)

The gte-large results offer a clearer and more compelling validation of dynamic head specialization switching. Head 10 served as the definitive initial-step specialist (Contribution: 0.43, Use Rate: 0.85 at Step-1). Crucially, Head 6 and Head 12 collectively assumed the role of long-range dependency specialists in later stages. Head 6’s contribution increased significantly at Step-4 (from 0.13 to 0.31), marking a clear functional transition. Most notably, Head 12 achieved a maximum Hit Rate of 0.50 at Step-4, despite minimal involvement at Step-1 (Contribution: 0.06). This sharp contrast in activation profiles unequivocally demonstrates the learned non-substitutability of specialized heads,

confirming that ParallaxRAG successfully engineers a task-adaptive retrieval architecture irrespective of the foundational text encoder.

Table 5: End-to-End QA Performance with Alternative Backbone Encoders using Llama3.1-8B as KGQA generator

Encoder	WebQSP		CWQ	
	Macro-F1	Hit	Macro-F1	Hit
E5	69.23	85.63	44.59	53.95
GTE	69.75	85.92	47.12	57.48

C.3.3 Correlation with Performance

The observed specialization patterns strongly correlate with end-to-end performance, particularly on the long-chain reasoning CWQ benchmark (Table 5). The GTE model, which exhibited a more pronounced dynamic specialization, significantly outperforms the E5 model on CWQ (Macro-F1: 47.12 vs. 44.59; Hit Rate: 57.48 vs. 53.95). Performance on the simpler WebQSP task is comparable (Macro-F1 difference is 0.52). This evidence supports the conclusion that the degree of functional specialization learned by the backbone encoder is a critical factor for robustness in multi-hop KGQA.

C.4 Head Specialization Verification Details

C.4.1 Linear Probing

To quantitatively verify that different attention heads specialize in distinct reasoning stages, we conducted a linear probing experiment. For each reasoning step, we aggregated the output scores from all attention heads to form a feature vector. A logistic regression classifier was then trained on these features to decode the current step number (from 1 to 4). Evaluated under 5-fold cross-validation grouped by sample, the classifier achieved a decoding accuracy that significantly outperformed a random baseline. This result confirms that the activation patterns of the attention heads contain sufficient information to distinguish between different stages of the reasoning process, supporting the hypothesis of functional specialization.

C.4.2 Difference in Difference in Difference

To causally validate the functional importance of specialist heads, we designed a Triple-Difference (DDD) intervention. This analysis isolates the additional performance degradation from ablating specialist heads versus random heads on long-hop

(> 1 -hop) questions, relative to short-hop (1-hop) questions. We first compute the Difference-in-Differences (DID) for both the specialist-ablation (DID_{spec}) and random-ablation (DID_{rand}) scenarios. The final causal estimate is then given by the Triple-Difference: $DDD = DID_{spec} - DID_{rand}$. Our experiment yielded a statistically significant DDD estimate, confirmed via bootstrap confidence intervals and permutation tests. This provides strong causal evidence that specialist heads are functionally non-substitutable and disproportionately crucial for complex, multi-hop reasoning.

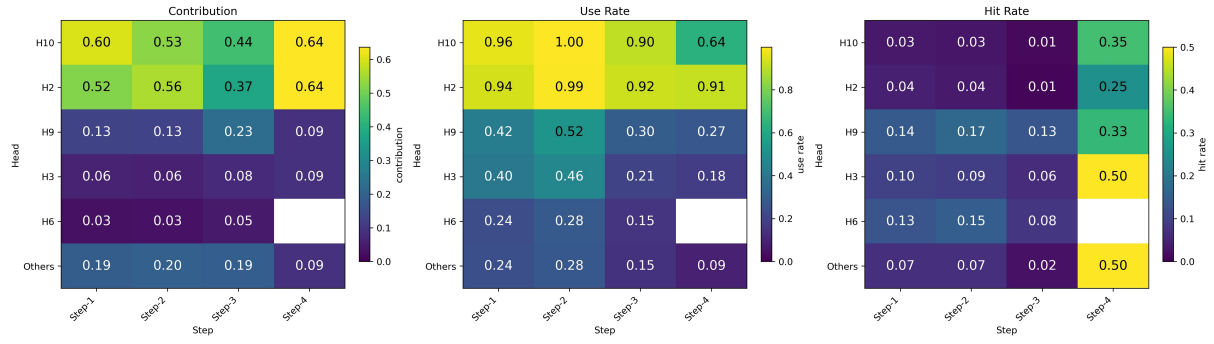
D Case Study

We present several representative cases from the CWQ dataset to demonstrate ParallaxRAG’s efficacy in multi-hop question answering, emphasizing its refined subgraph construction, reduced hallucinations, and robust handling of constraints through multi-view decoupling and head specialization.

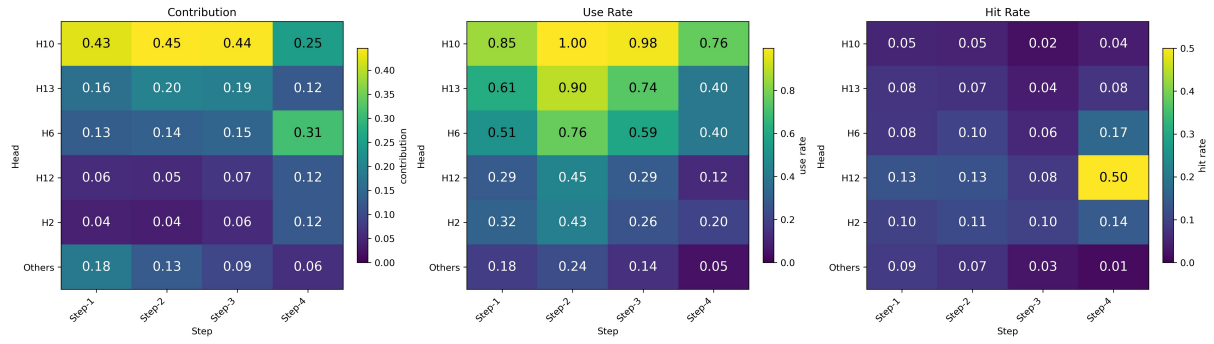
Case 1 (Figure 7): Single-Vector RAG retrieves a noisy subgraph, incorrectly following the containment path (*Nijmegen, ..., Netherlands*) while ignoring the adjacency constraint to France, thus outputting *Netherlands*. This failure highlights how its undifferentiated embeddings struggle to enforce multiple constraints. In contrast, ParallaxRAG’s multi-view retrieval isolates the correct evidence path: (*Nijmegen, nearby_airports, Weeze Airport*), (*Weeze Airport, containedby, Germany*), and (*Germany, adjoins, France*). By decoupling and prioritizing geographic constraints, it correctly answers *Germany*.

Case 2 (Figure 8): Single-Vector RAG’s flat representation fails to manage two distinct constraints (symbol and bisection). It retrieves a diffuse subgraph, conflates relations, and incorrectly links the Ring-necked Pheasant to Missouri, thus outputting *Missouri*. ParallaxRAG, however, uses constraint-specific heads to retrieve precise and separate facts: (*Ring-necked Pheasant, official_symbol_of, South Dakota*) and (*South Dakota, partially_contains, Missouri River*). This decomposition allows it to satisfy both constraints and correctly identify *South Dakota*.

Case 3 (Figure 9): For this simple transitive query, Single-Vector RAG retrieves sufficient facts, enabling the downstream LLM to correctly infer all three championship years. However, ParallaxRAG’s multi-head architecture retrieves ad-



(a) E5-large-v2 on CWQ dataset



(b) GTE-large on CWQ dataset

Figure 5: Attention Head Specialization Analysis on CWQ Dataset with Alternative Backbone Encoders. (a) Results using the E5-large-v2 model. (b) Results using the GTE-large model.

ditional constraint-related triples that create conflicting signals for the LLM. The diverse, multi-faceted evidence from different attention heads introduces competing interpretations that overwhelm the LLM’s reasoning process. Instead of performing the straightforward transitive inference, the LLM becomes paralyzed by the abundance of potentially relevant but ultimately distracting contextual information, incorrectly concluding that an answer cannot be determined and outputting None. This case exposes a limitation of our approach: while multi-head retrieval excels at complex multi-hop reasoning, it can inadvertently hinder performance on simple queries where focused, minimal context would be more effective.

System Prompt

Based on the triplets from a knowledge graph, please answer the given question. Please keep the answers as simple as possible and return all the possible answers as a list, each with a prefix "ans:".

In-Context Learning (Few-shot) Examples

Triplets:

(Lou Seal,sports.mascot.team,San Francisco Giants)
(San Francisco Giants,sports.sports team.championships,2012 World Series)
(San Francisco Giants,sports.sports championship event.champion,2014 World Series)
(San Francisco Giants,time.participant.event,2014 Major League Baseball season)
(San Francisco Giants,time.participant.event,2010 World Series)
(San Francisco Giants,time.participant.event,2010 Major League Baseball season)
(San Francisco Giants,sports.sports team.championships,2014 World Series)
(San Francisco Giants,sports.sports team.team mascot,Crazy Crab)
(San Francisco Giants,sports.sports team.championships,2010 World Series)
(San Francisco Giants,sports.professional sports team.owner s,Bill Neukom)
(San Francisco Giants,time.participant.event,2012 World Series)
(San Francisco,sports.sports team location.teams,San Francisco Giants)
(San Francisco Giants,sports.sports team.arena stadium,AT&T Park)
(AT&T Park,location.location.events,2012 World Series)

...

Question:

What year did the team with mascot named Lou Seal win the World Series?

To find the year the team with mascot named Lou Seal won the World Series, we need to find the team with mascot named Lou Seal and then find the year they won the World Series. From the triplets, we can see that Lou Seal is the mascot of the San Francisco Giants. Now, we need to find the year the San Francisco Giants won the World Series. From the triplets, we can see that San Francisco Giants won the 2010 World Series and 2012 World Series and 2014 World Series. So, the team with mascot named Lou Seal (San Francisco Giants) won the World Series in 2010, 2012, and 2014. Therefore, the formatted answers are:

ans: 2014 (2014 World Series)
ans: 2012 (2012 World Series)
ans: 2010 (2010 World Series)

User Prompt

Triplets:

$(e_a, r_{ab}, e_b),$

$(e_c, r_{cd}, e_d),$

...

Question:

What ...?

Figure 6: Detailed prompt for LLM question-answering used in our experiments for all samples

WebQTrn-241_dfb6c97ac9bf2f0ac07f27dd80f9edc2

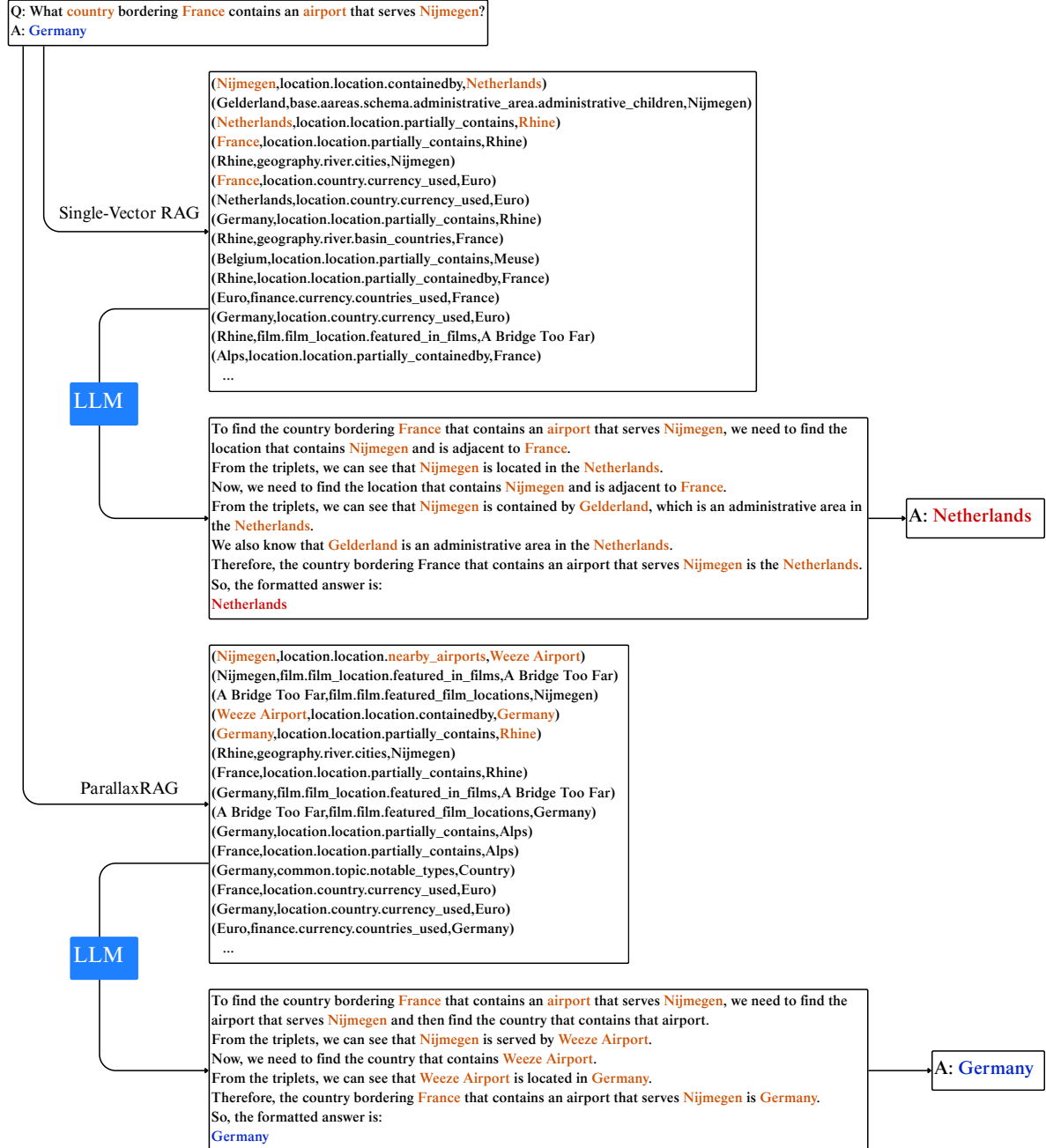


Figure 7: Comparison of retrieved subgraphs and reasoning chains for case WebQTrn-241

WebQTest-626_40c4288896adffe97901ff78149912e5

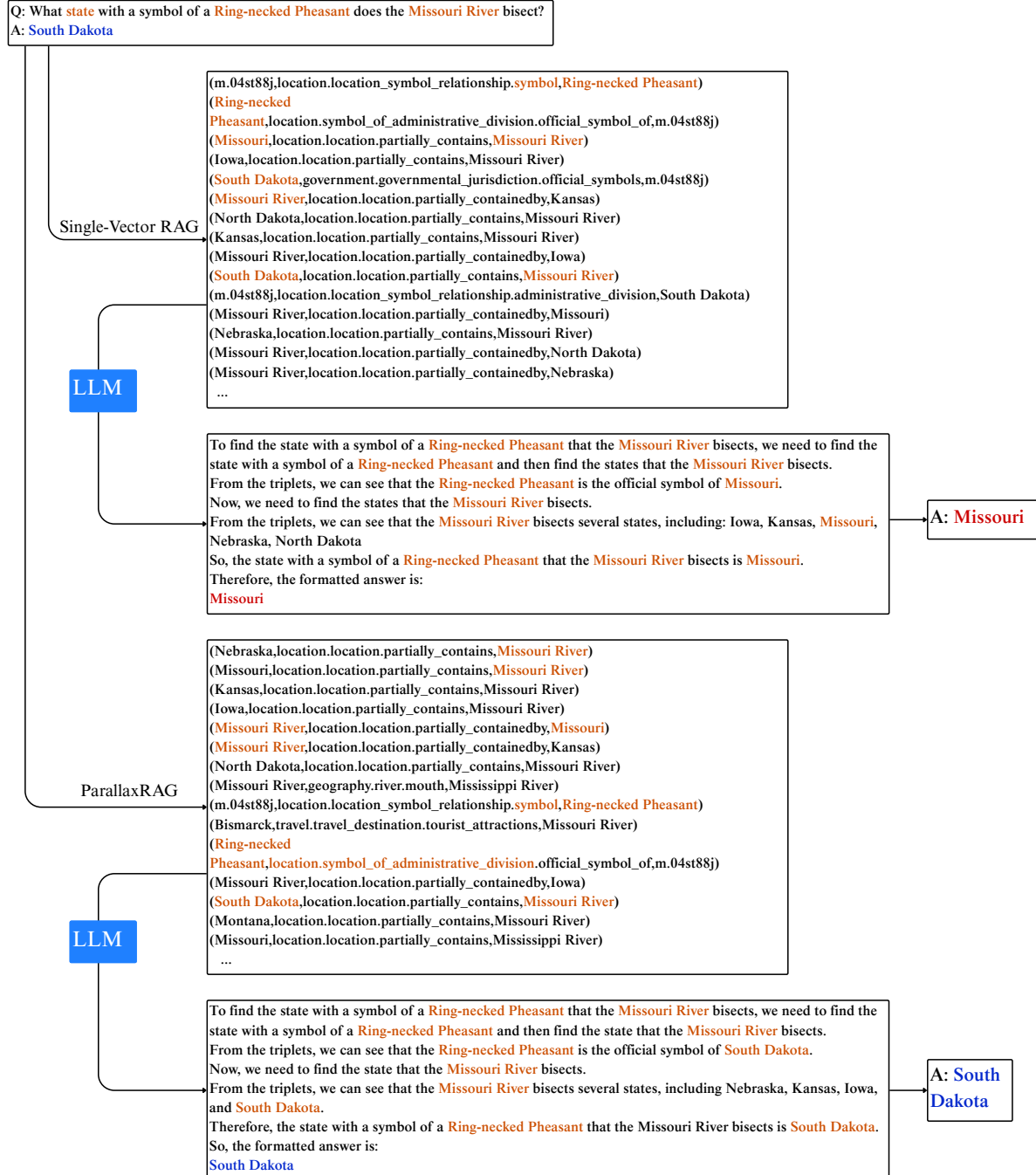


Figure 8: Comparison of retrieved subgraphs and reasoning chains for case WebQTest-626

WebQTrn-810_c334509bb5e02cacae1ba2e80c176499

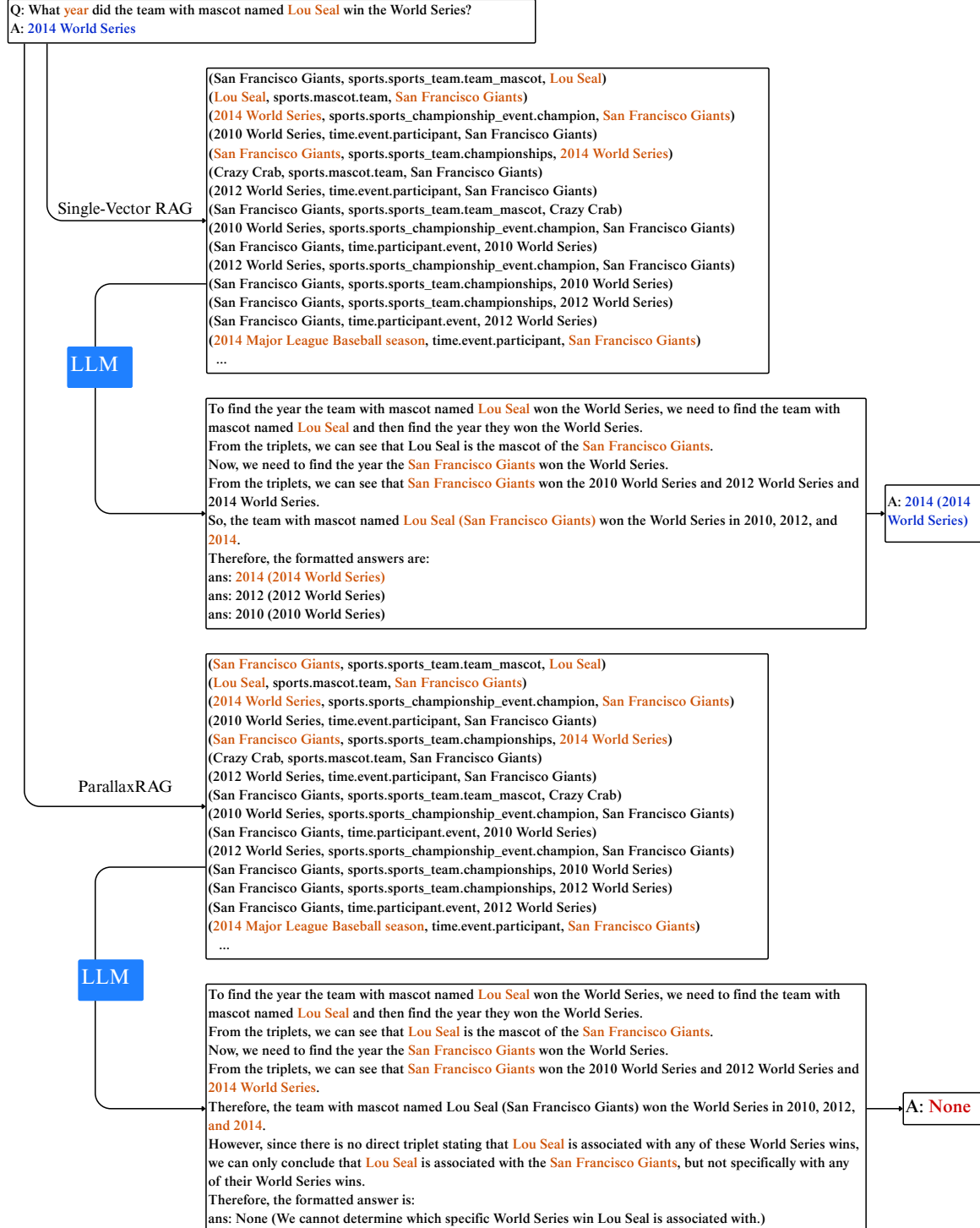


Figure 9: Comparison of retrieved subgraphs and reasoning chains for case WebQTest-810